

**OPTIMISATION OF QUALITY ASSURANCE
PROGRAMME (QAP) FOR IMAGE-GUIDED
ADAPTIVE RADIOTHERAPY (IGART)**

KASMAYANTI BINTI SAKARIA

UNIVERSITI SAINS MALAYSIA

2019

**OPTIMISATION OF QUALITY ASSURANCE
PROGRAMME (QAP) FOR IMAGE-GUIDED
ADAPTIVE RADIOTHERAPY (IGART)**

by

KASMAYANTI BINTI SAKARIA

Thesis submitted in fulfilment of the requirement

for the degree of

Master of Science

March 2019

ACKNOWLEDGEMENT

I would like to gratefully and sincerely thank my supervisor, Dr. Mohd Hafiz Bin Mohd Zin for his guidance, understanding, and patience. Without his assistance and dedicated involvement in every step throughout the process, this thesis would never have been accomplished. I also want to thank the staffs of Oncology and Radiotherapy Department, Advanced Medical and Dental Institute for giving me helpful advice and assistance. A special thanks to my family and friends for their constant support and encouragement in completing this project.

TABLES OF CONTENT

ACKNOWLEDGEMENT	ii
TABLES OF CONTENT	iii
LIST OF TABLES	vi
LIST OF FIGURES	vii
LIST OF ABBREVIATIONS	xii
ABSTRAK	xiv
ABSTRACT	xvi
CHAPTER 1 - INTRODUCTION	1
1.1 Introduction to modern radiotherapy	1
1.1.1 IMRT and IGRT techniques	2
1.1.2 IGART framework to overcome limitations in IG-IMRT	6
1.2 Quality assurance programme (QAP)	8
1.3 Challenges of QAP for IGART	10
1.4 Objectives of the study	11
1.5 Significance of the study	11
1.6 Thesis outline	12
CHAPTER 2 - LITERATURE REVIEW	13
2.1 Radiotherapy equipment	13
2.1.1 Components of a linac	14
2.1.2 Electronic portal device (EPID)	16
2.1.3 CBCT imaging system	17
2.2 Components of QAP for IGART	20
2.2.1 Linac dose output	21
2.2.2 Multileaf collimator (MLC) radiation shaping	23
2.2.3 CBCT image guidance system	24
2.3 Statistical process control	27

CHAPTER 3 - MATERIALS AND METHODS	30
3.1 Introduction	30
3.2 Specifications of linac	31
3.2.1 Multileaf collimator (MLC)	32
3.2.2 On-board image guidance systems	35
3.3 QA of the linac dose output	39
3.3.1 Measurement of reference output	40
3.3.2 Optimisation of linac output measurement	43
3.3.2(a) Evaluation of central axis dose output	45
3.3.2(b) Evaluation of beam flatness and symmetry	46
3.3.2(c) Evaluation of beam quality factor	48
3.3.3 Statistical process control analysis	48
3.4 QA of the MLC	50
3.4.1 Optimisation of the QA method to asses MLC performance	50
3.4.2 Analysis of MLC performance from the tracking data	52
3.4.3 Analysis of MLC performance from EPID image	56
3.5 QA of the CBCT image guidance system	58
3.5.1 Specifications of the CBCT phantoms	58
3.5.1(a) Catphan 600	59
3.5.1(b) CIRS 062QA	59
3.5.2 CBCT imaging parameters and acquisitions	63
3.5.2(a) Catphan 600	63
3.5.2(b) CIRS 062QA	63
3.5.3 Image analysis	65
3.5.3(a) Noise and uniformity	66
3.5.3(b) Contrast to noise ratio (CNR)	69
3.5.3(c) CT number accuracy	70
3.5.3(d) Low contrast visibility (LVC)	71
3.5.3(e) Spatial resolution	72
3.5.3(f) Geometric distortion	75
CHAPTER 4 - RESULTS AND DISCUSSION	76
4.1 Introduction	76
4.2 Performance of linac dose output	76
4.2.1 Central axis dose output	76
4.2.2 Beam flatness and symmetry	83
4.2.3 Beam quality	89
4.2.4 Statistical process control (SPC)	91

4.2.4(a) Central dose output	91
4.2.4(b) Beam flatness and symmetry	93
4.2.4(c) Beam quality	93
4.2.5 Summary of the linac dose output performance	96
4.3 Performance of dynamic MLC beam shaping	97
4.3.1 Results of MLC performance from the tracking data	97
4.3.2 Results of MLC performance from the EPID image	99
4.4 Performance of CBCT image guidance system	106
4.4.1 Noise and uniformity	106
4.4.2 Contrast to noise ratio (CNR)	112
4.4.3 CT number accuracy	114
4.4.4 Low contrast visibility	117
4.4.5 Spatial resolution	119
4.4.6 Geometric distortion	122
CHAPTER 5 - CONCLUSIONS AND RECOMMENDATION	124
5.1 Conclusions	124
5.2 Recommendations for future work	129
REFERENCES	131
APPENDIX	

LIST OF TABLES

		Page
Table 2.1	Relevant QAP for IGART	20
Table 3.1	Size of x-ray fields from combination of FOV and collimator cassette	39
Table 3.2	Tracked linac parameters by service graphing tool	52
Table 3.3	Imaging reconstruction parameters	65
Table 3.4	List of the measured metrics, the corresponding test module for Catphan 600 and CIRS 062QA and type of image reconstruction for each test module	66
Table 4.1	Range and mean \pm SD of the daily and monthly dose output measured from the two groups	80
Table 4.2	Comparison of maximum deviation of measured CT number against theoretical CT number obtained in this study and Gulliksrud et al. study	116
Table 5.1	Comparison between standard QAP in radiotherapy for IG-IMRT and optimised QAP in radiotherapy for IGART	128

LIST OF FIGURES

	Page	
Figure 1.1	Illustration of TCP and NTCP as a function of dose. Curve A represents TCP, curve B represents NTCP, and the therapeutic window is illustrated by the green shaded region	2
Figure 1.2	Illustration of (a) 3DCRT and (b) IMRT principle	4
Figure 1.3	Schematic diagram of target volumes delineation recommended by ICRU Report 62	4
Figure 1.4	IGRT process (top) and IGART process (bottom)	8
Figure 2.1	Typical assembly of modern linac with on board imaging system	13
Figure 2.2	Block diagram of the linac and rotating gantry head	14
Figure 2.3	Schematic diagram of cross-section of an a-Si EPID	17
Figure 2.4	X-ray tube and its power supply	18
Figure 2.5	Typical x-ray spectra	19
Figure 3.1	Linac, Elekta Synergy	32
Figure 3.2	Photograph of the multileaf collimator	33
Figure 3.3	Optical tracking mechanism for Elekta Agility	34
Figure 3.4	Interface of service graphing tool of the linac control system	34
Figure 3.5	Schematic diagram of three different FOV size: (a) small, (b) medium and (c) large	37
Figure 3.6	The nomenclature for the different directions related to the linac	38
Figure 3.7	Collimator cassette for small, medium and large FOVs (left to right): S20, M20, and L20. The last photograph is collimator cassette of M10	38
Figure 3.8	Setup of measurement absorbed dose to water under standard condition	41

Figure 3.9	Setup of monthly dose output measurement using ionisation chamber calibrated against SSDL	42
Figure 3.10	(a) Photograph of PTW Quickcheck and (b) Schematic diagram of Quickcheck	44
Figure 3.11	Setup of Quickcheck on treatment couch during daily measurement	45
Figure 3.12	Illustration of MLC positions during picket fence beam delivery	51
Figure 3.13	Raw data structure in the log file	54
Figure 3.14	(a) Service graphing setting tracking data and (b) Rearrangement of beam delivery parameters	55
Figure 3.15	Flowchart of the algorithm to generate fluence map of the tracking data	55
Figure 3.16	Conceptual diagram describe the difference between field edge (captured by the EPID) and leaf tip (tracked by the optical tracking)	57
Figure 3.17	Imaging test modules in Catphan 600	61
Figure 3.18	Test modules in CIRS 062QA	62
Figure 3.19	Catphan 600 setup on the treatment couch and the gantry angle rotated into -180°	64
Figure 3.20	CIRS 062QA setup on the treatment couch and the gantry angle rotated into -180°	64
Figure 3.21	(a) CTP486 and (b) uniformity test modules	67
Figure 3.22	(a) CTP486 and (b) uniformity test modules	68
Figure 3.23	(a) CTP404 and (b) CT number linearity test module	70
Figure 3.24	(a) CTP528 and (b) spatial resolution test module	74
Figure 3.25	Line pairs in (a) CTP528 and (b) spatial resolution test modules	74
Figure 3.26	(a) CTP404 and (b) magnification test modules	75
Figure 4.1	The percentage difference of dose delivered against calibration during monthly measurements using ionisation chamber	77

Figure 4.2	The percentage difference of dose delivered against calibration during daily measurements using Quickcheck	79
Figure 4.3	The percentage difference of dose output against calibration for monthly and daily measurements	79
Figure 4.4	Scatter plot of (a) 6 MV and (b) 10 MV beams during daily and monthly measurements	82
Figure 4.5	The boxplot of beam flatness deviation against calibration for 6 MV and 10 MV beams over 19 months	83
Figure 4.6	Histogram of beam flatness deviation against calibration of (a) 6 MV and (b) 10 MV beams	84
Figure 4.7	Beam symmetry deviation against calibration of 6 MV and 10 MV beam at (a) G-T and (b) L-R directions	86
Figure 4.8	Relative dose measured for 6 MV at (a) gun-target and (b) left-right chambers in the Quickcheck	87
Figure 4.9	Relative dose measured for 10 MV beam at (a) gun-target and (b) left-right chambers in the Quickcheck	88
Figure 4.10	The results of beam quality deviation against calibration of 6 MV and 10 MV beams during monthly measurement	89
Figure 4.11	The boxplot of beam quality deviation against calibration of 6 MV and 10 MV beams during daily measurement	90
Figure 4.12	Process behaviour chart of daily dose output for (a) 6 MV and (b) 10 MV beams	92
Figure 4.13	Process behaviour chart of beam flatness and symmetry for (a) 6 MV and (b) 10 MV beams	94
Figure 4.14	Process behaviour chart of beam quality for (a) 6 MV and (b) 10 MV beams	95
Figure 4.15	Fluence maps reconstructed from optical tracking data from delivering of picket fence beam at gantry angle 0°	97
Figure 4.16	Profile plot across each leaf in the fluence map of optical tracking (this figure shows leaf number 40) and shows the gap size measurement at point where the amount of MU is higher than 2 MU	98
Figure 4.17	Histogram plot showing the gap size measured from optical tracking data	99

Figure 4.18	Fluence maps reconstructed from EPID image from delivering of picket fence beam at gantry angle 0°	100
Figure 4.19	(a) Fluence map of EPID in grey scale, (b) determination of individual leaf from the peak, (c) filtering image with canny filter, (d) high contrast image, and (e) beam profile across cross plane of each individual leaf	101
Figure 4.20	Histogram plot showing the gap size measured from EPID	102
Figure 4.21	Boxplot of gap size difference measured from optical tracking and EPID at four nominal gantry angles	104
Figure 4.22	Histogram plot showing the gap size difference measured from the optical tracking and EPID	104
Figure 4.23	RMS of gap size difference measured from EPID and optical tracking leaf-by-leaf	105
Figure 4.24	Leaf-by-leaf variation of RMS of gap size difference measured from optical tracking and EPID at four nominal gantry angles	106
Figure 4.25	Intensity profile across horizontal and vertical ROIs in (a) CTP428 and (b) uniformity test modules	107
Figure 4.26	Fitted lines of intensity profile for every month using second degree of polynomial equation across horizontal and vertical ROIs in (a) CTP428 and (b) uniformity test modules	108
Figure 4.27	UNI values obtained from Catphan 600 and CIRS 062QA for 6 months	110
Figure 4.28	The scatter plot of INU at horizontal and vertical directions measured by Catphan 600 and CIRS 062QA. The R value shown in the denotes correlation coefficient value	110
Figure 4.29	UI measured from Catphan 600 and CIRS 062QA for 6 months	111
Figure 4.30	The scatter plot of UI measured from Catphan 600 and CIRS 062QA. The R value denotes correlation coefficient value	112
Figure 4.31	CNR values of every insert in the CTP404 and CT number linearity test modules	113
Figure 4.32	Scatter plot of CNR values of every inserts in Catphan 600 and CIRS 062QA	114
Figure 4.33	CT number calibration obtained from first month data	115
Figure 4.34	CT number measured from Catphan 600 and CIRS 062QA for six months	115

Figure 4.35	Measured CT number against theoretical CT number of each insert in Catphan 600 and CIRS 062QA	116
Figure 4.36	Scatter plot of CT number measured from Catphan 600 and CIRS 062QA. The R refers the correlation coefficient	117
Figure 4.37	Low contrast visibility measured from Catphan 600 and CIRS 062QA over 6 months	118
Figure 4.38	The scatter plot and correlation coefficient of LCV measured from Catphan 600 and CIRS 062QA	119
Figure 4.39	Spatial resolution of Catphan 600 and CIRS 062QA	120
Figure 4.40	Spatial frequency at f_{50} and f_{10} of Catphan 600 and CIRS 062QA	121
Figure 4.41	The scatter plot and correlation coefficient of spatial frequency at f_{50} and f_{10} measured from Catphan 600 and CIRS 062QA	121
Figure 4.42	Geometric distortion measured at (a) horizontal and vertical directions in CTP404 of Catphan 600, and (b) horizontal, vertical and angle 225° directions in magnification module test of CIRS 062QA	123

LIST OF ABBREVIATIONS

2D	two dimensional
3D	three dimensional
3DCRT	three dimensional conformal radiotherapy
a-Si	amorphous silicon
AAPM	American Association of Physicists in Medicine
ACMP	American of College of Medical Physics
ASTRO	American Society of Radiation Oncology
CAT	customer acceptance testing
CBCT	cone beam computed tomography
CNR	contrast to noise ratio
CT	computed tomography
CTV	clinical tumour volume
EFOMP	European Federation of Organisations for Medical Physics
EPID	electronic portal imaging device
ESTRO	European Society for Radiotherapy and Oncology
FPD	flat panel detector
GTV	gross tumour volume
IAEA	International Atomic Energy Agency
ICRU	International Commission on Radiation Unit and Measurements
IEC	International Electrochemical Commission
IGART	image-guided adaptive radiotherapy
IGRT	image-guided radiotherapy
IMRT	intensity modulated radiotherapy
IPEM	Institute of Physics and Engineering in Medicine

ITV	internal target volume
kV	kiloVoltage
LCV	low contrast visibility
linac	linear accelerator
MLC	multileaf collimator
MRI	magnetic resonance imaging
MTF	modulation transfer function
MU	monitor unit
MV	mega voltage
NPC	nasopharyngeal carcinoma cancer
NTCP	normal tissue complication
OAR	organ at risk
PDD	percentage depth dose
PET	positron emission tomography
PTV	planning target volume
QAP	quality assurance programme
RMS	root mean square
ROI	region of interest
SAD	source to axis distance
SPC	statistical process control
SSD	source to surface distance
TCP	tumour control probability
TG	Task Group
TPR	tissue phantom ratio
TRS	Technical Report Series

PENGOPTIMUMAN PROGRAM JAMINAN KUALITI (QAP) UNTUK RADIOTERAPI ADAPTIF BERPANDUKAN IMEJ (IGART)

ABSTRAK

Radioterapi adaptif berpandukan imej (IGART) adalah rawatan termaju yang melibatkan proses mengubah suai perancangan rawatan dengan mengambil kira perubahan pada isipadu tumor sepanjang rawatan. Kajian ini bertujuan untuk mengoptimumkan program jaminan kualiti (QAP) terhadap linac yang berkaitan dengan IGART. Linac dikaji dalam penyelidikan ini adalah Elekta Synergy yang mempunyai 80 pasang kolimat pelbagai lapisan dinamik (MLC) dan sistem berpandu imej tomografi terkompulasi pancaran kon (CBCT). Prestasi linac diukur menggunakan QAP yang telah dioptimumkan dari segi penyampaian pengeluaran dos, MLC dinamik dan sistem berpandu imej CBCT. Pengeluaran dos linac untuk pancaran 6 MV dan 10 MV diukur setiap hari menggunakan alat pengesan dos yang telah ditentukan iaitu Quickcheck. Parameter yang dinilai selama 19 bulan adalah dos pusat, kesamarataan, kesimetrian dan kualiti pancaran. Variasi keputusan berada pada julat toleransi iaitu pusat dos $\pm 2\%$, kesamarataan pancaran $\pm 1.5\%$, kesimetrian pancaran $\pm 3\%$ dan kualiti pancaran $\pm 3\%$. Prestasi MLC dinamik dianalisis secara mingguan dari segi ketepatan kedudukan kolimat menggunakan sistem pemantau MLC pada Elekta dan disahkan dengan teknik piawai menggunakan EPID. Julat ralat kedudukan MLC dinilai dari sistem pemantauan MLC adalah -0.30 mm hingga 0.80 mm, ianya berada dalam julat keputusan dari imej EPID. Prestasi sistem berpandu imej CBCT dinilai setiap bulan dari segi kualiti imej dan ketetapan nombor CT menggunakan phantom CIRS 062QA yang bersaiz kecil dan dibandingkan dengan pengukuran menggunakan phantom Catphan 600. Terdapat variasi antara phantom tetapi kedua-duanya mempunyai trend yang sama sepanjang tempoh 6 bulan. Variasi wujud disebabkan oleh perbezaan saiz dan reka bentuk phantom. Secara kesimpulan, QAP

yang telah dioptimumkan adalah lebih cekap kerana memerlukan penyediaan yang lebih mudah untuk mengukur beberapa parameter dalam satu masa, keputusan yang diperolehi juga adalah sama dengan keputusan daripada teknik piawai QAP. Maka, QAP yang dioptimumkan boleh dijalankan secara rutin dan lebih kerap untuk memberikan jaminan keselamatan dalam rawatan teknik IGART.

OPTIMISATION OF QUALITY ASSURANCE PROGRAMME (QAP) FOR IMAGE-GUIDED ADAPTIVE RADIOTHERAPY (IGART)

ABSTRACT

Image-guided adaptive radiotherapy (IGART) is an advanced radiotherapy treatment technique that involves treatment plan modifications during the treatment course to account for temporal changes in tumour volume. The purpose of this study is to develop a Quality Assurance Programme (QAP) for a linac that is optimised for IGART. The linac investigated in this study is an Elekta Synergy linac with 80 pairs of multileaf collimators (MLC) and cone beam computed tomography (CBCT) image guidance system. An optimised QAP was developed to assess relevant linac performance parameters including dose output delivery, dynamic MLC and CBCT image guidance system. Linac dose output was measured daily using a cross-calibrated detector, Quickcheck. The parameters evaluated were central dose output, beam flatness, beam symmetry and beam quality for a period of 19 months. The variations of measurement were within the tolerance level. The central dose outputs are within $\pm 2\%$, the beam flatness results are within $\pm 1.5\%$, the beam symmetry results are within $\pm 3\%$ and the beam quality results are within $\pm 3\%$. The dynamic MLC performance was analysed weekly in term of leaf positional accuracy using Elekta's propriety MLC tracking system that is verified against EPID measurement. The MLC position errors tracked were between -0.30 mm to 0.80 mm, within the range of the results from EPID. The performance of CBCT image guidance system was assessed monthly in term of image quality and CT number accuracy using smaller sized CIRS 062QA and compared against the more commonly used Catphan 600. The interphantom variations were observed in the measured parameters, yet they have similar trend to each other. The variations exist due to the difference in the size and geometric design of the phantoms. In conclusion, the optimised QAP developed was

more efficient that provides a simpler setup procedure for multiple measurement and semi-automated analysis, but also agreed with the results obtained using standard QAP method. Thus, the optimised QAP can be performed routinely at higher frequency to provide a safety net for IGART delivery.

CHAPTER 1 INTRODUCTION

1.1 Introduction to modern radiotherapy

Malaysian National Cancer Registry Report (MNCR) reported a total of 103507 new cancer cases diagnosed in Malaysia during the period of 2007 to 2011 (Zainal & Nor Saleha, 2011). Radiotherapy is one of the most common types of cancer treatment, either as a standalone treatment or in combination with chemotherapy and/or surgery. Radiotherapy is used for the treatment of malignant tumours and plays an important part in cancer cure by delivering ionising radiation.

The main goal of radiotherapy is to deliver radiation dose to the tumour whilst minimising the dose to normal tissue. Radiation traverses through the body to reach cancerous tissue. Some normal tissues are exposed to the radiation with magnitude depending on the type and the amount of radiation. This is described by the tumour control probability (TCP) and normal tissue complication probability (NTCP) curves illustrated in Figure 1.1. TCP is shown by curve A, while NTCP is shown by curve B and the green shaded region illustrates the therapeutic window, which highlights a range of doses for which there is an acceptable balance between the probability of cure and the risk of excessive toxicity. Increasing the dose beyond this range improves local control, but at the cost of increasing the risk of normal tissue complications. Hence, conformal treatment plans are required to obtain the highest curative probability and at the same time the lowest complication probability.

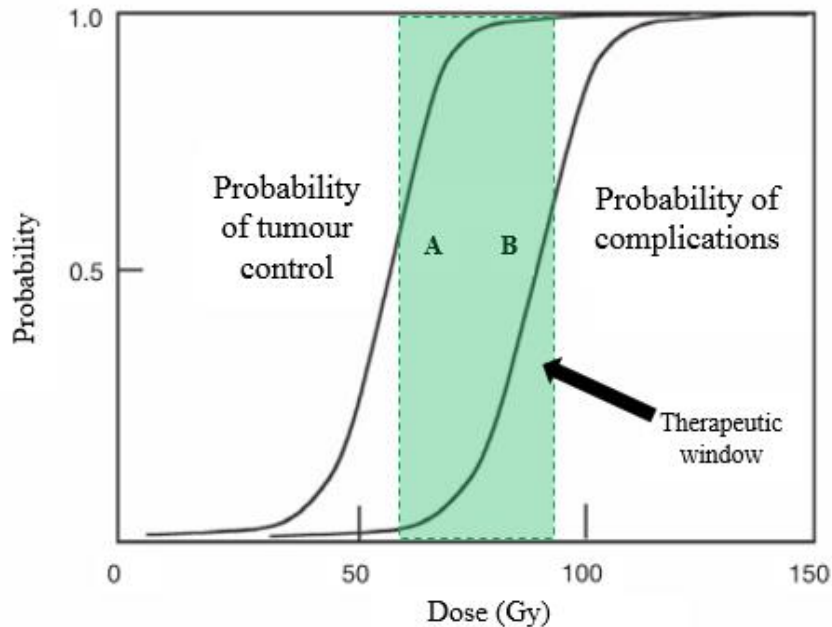


Figure 1.1 Illustration of TCP and NTCP as a function of dose. Curve A represents TCP, curve B represents NTCP, and the therapeutic window is illustrated by the green shaded region (Rosenberg, 2008)

Recent advances in radiotherapy technology has allowed delivery of more conformal radiation to achieve the aim of radiotherapy. This will be addressed in the subsequent sections. Section 1.1.1 will explain current treatment techniques using intensity modulated radiotherapy (IMRT) and image guided radiotherapy (IGRT) and Section 1.1.2 will describe image-guided adaptive radiotherapy (IGART) technique.

1.1.1 IMRT and IGRT techniques

IMRT is a sophisticated treatment technique widely used today, with a complex treatment chain to enable delivery of highly conformal beam dose to the patients. The basic principle of IMRT is to use modulated beam intensities to vary the dose delivery and irradiating the tissue from different directions to maximise dose at beam intersections. IMRT improves target coverage and organ at

risk (OAR) sparing compared to conventional three dimensional conformal radiotherapy (3DCRT) treatment technique (Van Dieren et al., 2000; Xia et al., 2000).

3DCRT is based on 3D anatomic information such that resulted dose distribution conforms to the target volume closely in term of adequate dose to the tumour and minimal dose to the normal tissues. The treatment plan in 3DCRT is manually optimised to obtain the desired dose distribution. The beam parameters such as number of beams, beam directions, beam shapes, wedges and weightages are set, then the computer calculates the resulting dose distribution. For IMRT treatment plan, it is the other way around, where the physicist only has to decide the desired dose distributions and some of the treatment parameters. The rest of the treatment parameters are calculated by the computerised treatment planning system. The radiation intensity in 3DCRT is uniform within each beam, whilst modulated in IMRT. The principles of 3DCRT and IMRT treatment technique is illustrated in Figure 1.2 (a) and (b), respectively.

In IMRT, target volumes and organ at risks (OARs) are delineated following the recommendations by ICRU Report 62 (ICRU, 1999), as shown in Figure 1.3. The target volumes to be considered while delineating are the gross tumour volume (GTV), clinical tumour volume (CTV), internal target volume (ITV) and planning target volume (PTV). GTV is contoured based on the gross radiologically visible tumour during treatment planning. Then other target volumes are expanded relative to GTV. CTV is a volume of tissue that contains GTV and/or subclinical malignant diseases, ITV is the uncertainties of CTV due to the internal organ motion, and PTV is a geometrical extension of CTV to account for all geometrical variations and inaccuracies. The OARs are the normal tissues surrounding the target volume that are critical structures to be spared from the radiation dose during treatment delivery.

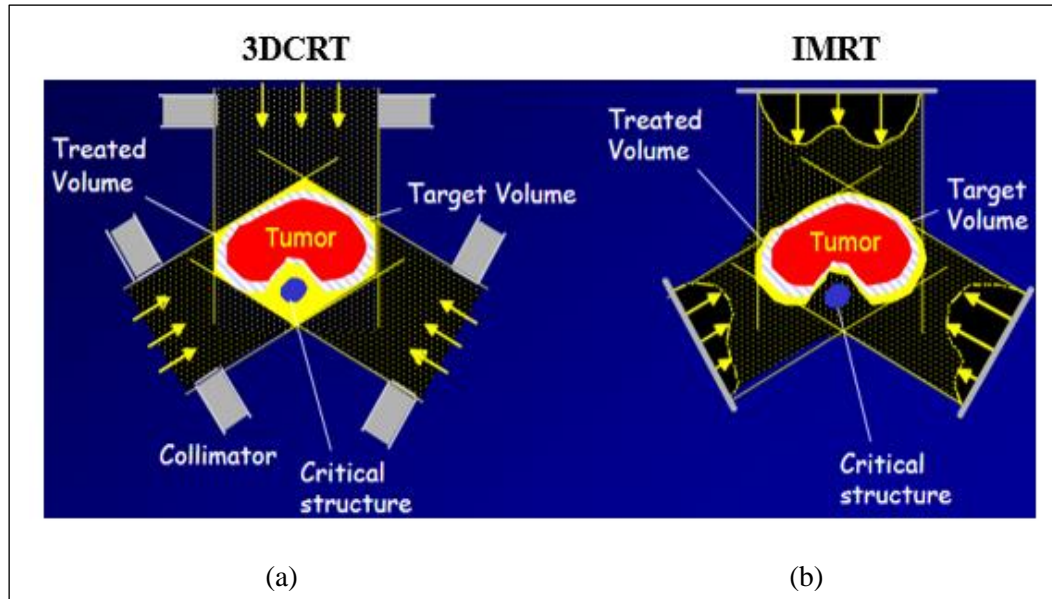


Figure 1.2 Illustration of (a) 3DCRT and (b) IMRT principle. Image taken from Schlegel et al. (Schlegel & Mahr, 2007)

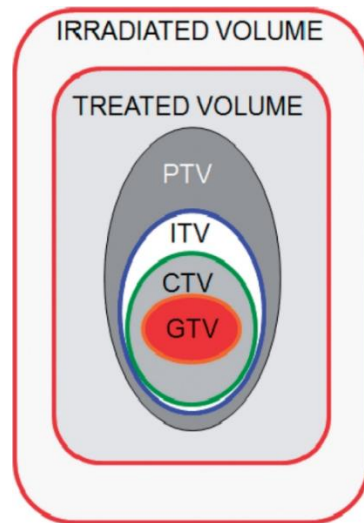


Figure 1.3 Schematic diagram of target volumes delineation recommended by ICRU Report 62 (ICRU, 1999)

There are many studies performed to demonstrate how IMRT can improve tumour irradiation while sparing the surrounding normal tissues (Jin et al., 2009; Zhang et al., 2013). Lee et al. has studied the impact of IMRT field in the treatment of 67 patients for nasopharyngeal carcinoma (NPC) cancer. The patients were followed-up over 7 to 72 months for physical

examination, and obtained the baseline post-treatment MRI scan and positron emission tomography (PET) scan of the nasopharynx and neck. They found that IMRT provides excellent tumour target coverage and allowed the delivery of a high dose to the target with significant sparing of the salivary glands and other nearby critical normal tissues (Lee et al., 2002).

The highly conformal IMRT dose distributions are more sensitive to misalignments of the target with respect to the planned dose. Geometric uncertainties may arise that can affect the accuracy and precision of IMRT treatment (Dawson & Sharpe, 2006). The geometrical uncertainties can occur in term of patient setup and organ motions. The steep dose gradients from the IMRT treatment particularly are very sensitive to the patient position errors and anatomic changes. Small changes in anatomic of the patient can result in under-dosing the target volumes and overdosing the healthy tissues, which may translate into compromised tumour control and/or increased adverse effects (Wu et al., 2011).

Minimising these uncertainties by guidance from on board imaging system can improve IMRT treatment delivery. The common image-guidance used are electronic portal device (EPID) and cone-beam computed tomography (CBCT). This process is known as image guided radiotherapy (IGRT) that can be defined as the use of frequent imaging in the treatment room prior to the beam delivery. The development of IGRT enables imaging of the tumour before IMRT treatment delivery. The treatment position is verified based on the position on-treatment image relative to the CT scan image thus enable reduction of errors that could occur during treatment. The patient setup error is corrected based on the acquired images. Nabavizadeh et al. has done a survey regarding the practice of IGRT on radiotherapy workflow. Out of 601 respondents of American Society of Radiation Oncology (ASTRO), 95% reported IGRT use in the radiotherapy workflow and also 92% of them used CBCT imaging for all treatment sites except breast cancer (Nabavizadeh et al., 2016).

1.1.2 IGART framework to overcome limitations in IG-IMRT

The accuracy and precision of IMRT treatment delivery can be improved by IGRT. However, one of the main limitations in IGRT is the way that anatomical changes are dealt with. Several researchers have investigated the changes occurred during the course of treatment. Barker et al. reported the changes in GTV in the head and neck cancer over the course of radiotherapy by obtaining three CT scans per week for 14 patients. The GTV decreased throughout the course of treatment at a median rate of 0.2 cm^3 per treatment day, resulting in a median total GTV loss of 70% of the first fraction (Barker et al., 2004). Besides, Wang et al. studied an average volume loss of 20% at parotid glands after three weeks treatment (Wang et al., 2009).

IGRT technique relies on initial imaging radiotherapy simulation and treatment planning, and the following fractions only required correction of patient positioning before dose delivery (Xing et al., 2011). In fact, the changes either in size, shape or position of the tumour or OARs since the initial planning CT cannot be corrected only by patient positioning and/or treatment couch shifts (Schwartz, 2012), unless adapting treatment plan during the course of treatment (Mohan et al., 2005).

Image guided adaptive radiotherapy (IGART) was first introduced by Yan et al., which is an approach to correct for daily and normal tissue variations through modification of original treatment plan during the course of treatment (Yan et al., 1997). There are several researchers that have investigated the benefit of IGART in clinical implementation. Nijkamp et al. has studied the first clinical implementation of IGART for 20 prostate patients using CBCT imaging. The irradiated target volume safely reduced by 29% and thus lead to a significant reduction in the dose to the rectum (Nijkamp et al., 2008). Clinical benefit of re-planning was also assessed by Jensen et al., where adaptive radiotherapy in IMRT of head and neck tumours have been conducted for 15 patients. The results showed that re-planning during the course of IMRT treatment maintains

adequate coverage of the target volumes and allows parotid gland sparing (Jensen et al., 2012). A recent study by Keall et al. treated eight prostate patients using IGART treatment technique. They found that the dose distribution from IGART is closer to the planned dose than without IGART. For the largest motion fraction, CTV received 100% of the prescribed dose with IGART treatment, meanwhile, CTV only received 95% of the prescribed dose without IGART (Keall et al., 2018). Moreover, Allen et al. also proved that the use of IGART strategy on patients treated with IMRT for head and neck cancer reduced the incidence of high-grade skin toxicity and mucositis in the acute setting (Chen et al., 2017).

IGART approaches break the conventional sequential procedure of radiotherapy simulation, treatment planning, patient shift (after position verification) and dose delivery as illustrated in Figure 1.4. IGART involves dose distribution and imaging assessment throughout the course of treatment to determine the needs of plan modification prior to treatment delivery (Xing et al., 2011). The decision on treatment plan modification is based on the anatomical changes measured from the on-board imaging system. The initial treatment plan is modified when anatomical changes alter the dose distribution to the extent that treatment planning criteria are no longer met by under-dosage of the target volumes and/or over-dosage the OARs.

Theoretically, IGART can be performed in three different timescales: offline between fractions, online immediately prior to a fraction or real time during the fraction. The offline technique involves delivering future treatment fraction from the adaptation of treatment plan based on the previous fraction. Meanwhile, the online technique involves adapting treatment plan based on image acquired from the current fraction. Lastly, real time technique involves continually updating the treatment based on images obtained simultaneously with treatment, such as the target tumour occurs in the chest or abdomen which affected by respiratory or other source of intra-fraction motion (Furlow, 2016; Keall et al., 2010; Kupelian & Sonke, 2014).

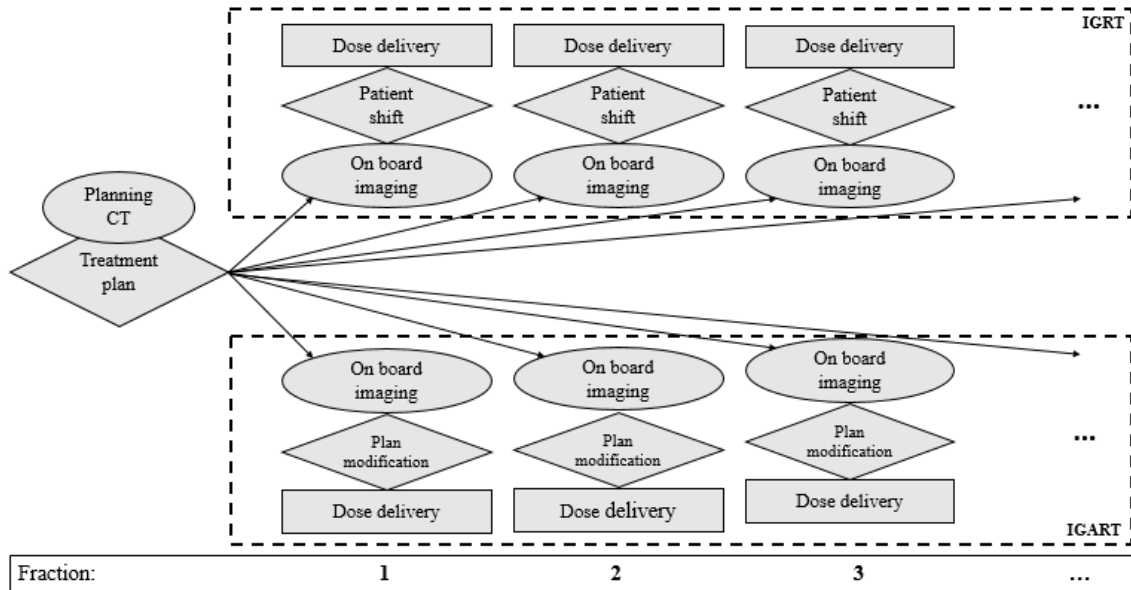


Figure 1.4 IGRT process (top) and IGART process (bottom) (Timmerman & Xing, 2012)

1.2 Quality assurance programme (QAP)

Advances in IMRT and IGRT delivery technologies throughout the last decade have made it possible to deliver highly conformal plan by modulating the beam intensity to adapt the changes on the tumour target using IGART. Therefore, robust quality assurance programme (QAP) is required to ensure the consistency of machine performance from the time of commissioning and customer acceptance testing (CAT) (Nath et al., 1994). There are several international recommendations on procedures and conditions for commissioning and CAT, such as from The International Electrotechnical Commission (IEC), American Association of Physicists in Medicine (AAPM), and American of College of Medical Physics (ACMP). The machine parameters obtained from the commissioning and CAT were set as baseline. The deviation of machine parameters from the baseline could affect the accuracy of radiotherapy treatment. The malfunctioning of the machine, mechanical breakdown, physical accidents, and hardware or component replacement may cause the deviation of machine parameters. According to World Health Organisation (WHO), QAP for radiotherapy is to minimise errors in treatment delivery and

thereby improves the results of therapy by increasing remission rates and decreasing complication and recurrence rates (World Health Organisation, 1988).

The guidelines for QAP for radiotherapy are mainly based on the national and international recommendations such as IEC, AAPM, IAEA and Institute of Physics and Engineering in Medicine (IPEM). Some of the guidelines described recommendation on test procedure, test frequencies and the tolerance level.

The technology of linac is rapidly evolving to assure the IGART delivery is precise and accurate. Hence, the QAP also need to be improved as the treatment will become more sophisticated. The delivery parameters must be accurately delivered and should be routinely monitored. For example, there were evolutions of recommendations of QAP for radiotherapy in the AAPM report. The recommendations started from the task group (TG)-13 (Baily et al., 1994), TG-40 (Kutcher et al., 1994), and the latest is TG-142 (Klein et al., 2009). TG-40 supersedes the recommendations of TG-13 and also TG-142 updated the recommendations of TG-40 report on quality assurance and added recommendations for the new ancillary delivery technologies in the linac, such as asymmetric jaws, multileaf collimation (MLC), dynamic/virtual wedges. TG-142 accomplished the update of TG-40 by specifying new tests, frequency of the tests, and the tolerances level. TG-142 also includes guidance that should be taken for the physicists to implement particular actions based on the tolerance level, whether they are inspection action, scheduled action or immediate stop treatment action.

TG-142 also described basic recommendation guidelines on test and tolerance for on board image-guidance system performance. AAPM TG-179 has updated TG-142 in providing comprehensive guidelines of QAP for commercial available of CT-based IGRT (Bissonnette et al., 2012). Recently, European Federation of Organisations For Medical Physics (EFOMP) in cooperation with IAEA and European Society for Radiotherapy and Oncology (ESTRO) have prepared a comprehensive guidelines to assess the image quality and radiation output in all types

of CBCT imaging system (Gala et al., 2017a). The report consists of detailed procedures of the image quality tests, the action levels and frequency of the tests.

Tests and measurements of the machine parameters must be performed periodically to ensure the mechanical, geometrical, dosimetry, image quality and general safety of the machine is maintained throughout use. The QAP is divided to daily, weekly, monthly and annually that cover all aspects of the machine performance tests. The daily tests are performed every morning to ensure daily optimum linac output. Monthly tests that is more complicated and often time consuming are an expansion of the basic daily check to include dosimetry, mechanical and multileaf collimator (MLC) performance of the linac and also the performance of image guidance system. Annual tests are typically subset of the tests performed during commissioning and CAT.

1.3 Challenges of QAP for IGART

IGART has become increasing popular radiotherapy treatment technique over the last two decades. Implementation of IGART in the clinical practice requires high levels of automation in term of image acquisition, registration, treatment dose construction, and adaptive planning optimisation. The increased complexity of IGART technique might create an environment in which treatment errors are prone to occur and QAP should be also improved and efficiently implemented (Yan, 2008). There are many literatures including articles, reports, and books that discussed the routine QA tests for IMRT and IGRT treatment. However, to the best of author's knowledge, the QAP specifically optimised for IGART treatment have not been addressed in detail in the literatures, except Yan and Wu et al. that have only defined the technical components of IGART treatment, such as image guidance, dose verification and treatment adaptation without recommendation of optimised protocols to improve the QAP efficiency (Wu et al., 2011; Yan, 2008). Therefore, this study aims to develop an optimised QAP based on the existing QA test

recommendations that are relevant for IGART treatment. The components involved will be further elaborated in Section 2.2.

1.4 Objectives of the study

The main objective of the study is to develop an optimised QAP for IGART. Two sub-objectives are as follows.

- To measure the radiotherapy machine parameters essentials for IGART
- To develop an optimised QAP for implementation of IGART

1.5 Significance of the study

Robust QAP plays an important role to ensure that the linear accelerator performance is within the specifications measured at the time of commissioning and customer acceptance testing. Development of a QAP specifically optimised for IGART treatment is necessary in order to have a safe treatment delivery of the complex IGART treatment to the patient. Besides, busy clinic and heavy workloads of the physicist justify the need for more efficient and reliable approaches to QAP but at the same time can measure the machine performance accurately and precisely over the time. Optimised QAP developed from this study is expected to be able to reduce the workloads by performing simpler QAP procedure and at the same time increase the confidence of IGART treatment delivery.

1.6 Thesis outline

This chapter has briefly explored the motivation of this work and has highlighted the need for development of QAP specifically optimised for complex IGART treatment delivery. Further details will be described in the next chapters. Chapter 2 explains the equipment of advanced radiotherapy system. This chapter also presents a review of literatures describing the components of QAP relevant for IGART treatment. Next, Chapter 3 describes the specifications of linac system investigated in this study. The equipment used and methods of performing the optimised QA procedure of the linac system will be demonstrated in this chapter. Chapter 4 presents the results of the QA described in Chapter 3. Chapter 5 summarises the optimised QAP for a linac that is relevant to ensure accurate delivery of IGART treatment. The recommendation for the future work will be also included in this chapter.

CHAPTER 2 LITERATURE REVIEW

2.1 Radiotherapy equipment

Radiotherapy is delivered using a linac. Advanced radiotherapy system includes on-board imaging system that is integrated on the linac. Figure 2.1 shows the typical assembly of a linac with on board imaging system. A linac consists of a rotating gantry, a gantry head, a movable treatment couch, a CBCT imaging system (kV source tube and kV flat panel) and an electronic portal device (EPID). Section 2.1.1 will explain the main components of a linac. Section 2.1.2 and 2.1.3 will explain the on-board imaging systems.

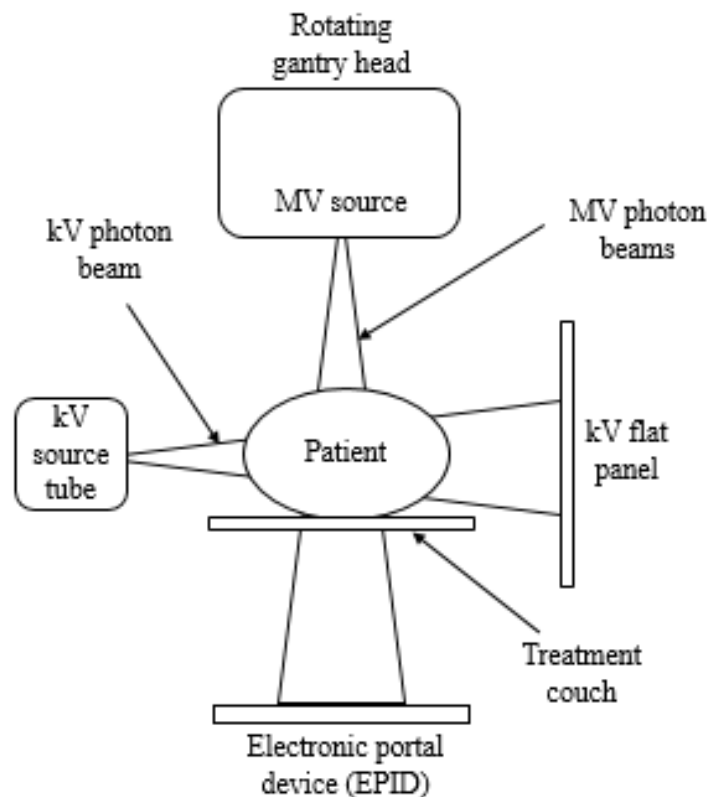


Figure 2.1 Typical assembly of modern linac with on-board imaging system

2.1.1 Components of a linac

High energy photon beams are generated from the linac as shown in Figure 2.2. Major components of a linac are the rotating gantry and the gantry head as illustrated in the figure. A power supply provides direct current (DC) power to the modulator. The pulsed modulator has a pulse forming network that converts the continuous electrical energy into pulse form. The pulses are simultaneously delivered to the magnetron and the electron gun. The injection of pulses into the magnetron causes the production of pulsed electromagnetic waves that are then injected into the accelerating waveguide. While, the injection of pulses into the electron gun resulting in a pulsed stream of electrons also entering the accelerating waveguide.

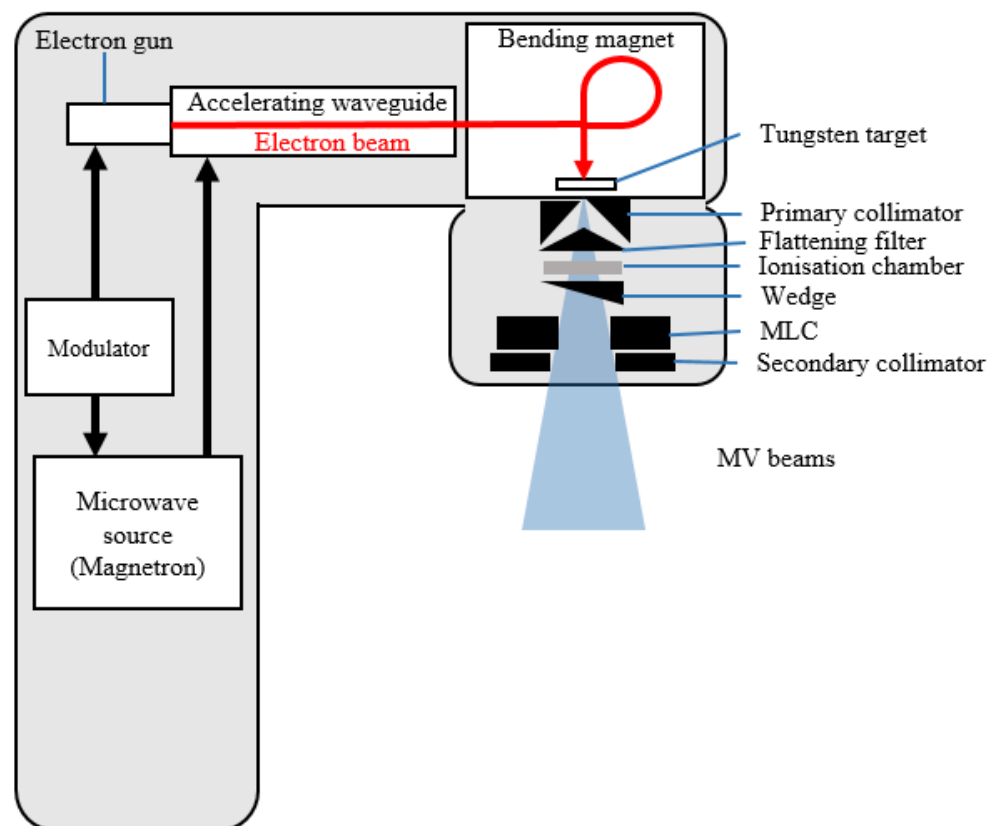


Figure 2.2 Block diagram of the linac and rotating gantry head. Diagram also shows the production of the MV beams

The tungsten filament cathode in the electron gun that is heated when voltage is applied. The electrons are then ejected from the filament. The heat applied on the filament controlled the number of ejected electrons. The electrons injected into the accelerating waveguide and interact with the pulsed electromagnetic waves then produced high energy electrons. The electron beams exit the accelerating waveguide and enter the bending magnet region that caused the electron beams to bend. This process ensure the electron beams strike the tungsten target and focuses to a diameter of 1 mm.

The photon beam is first collimated by a fixed primary collimator located below the tungsten target. The collimated beam then passes through the flattening filter that is responsible to modify narrow beam and creates a uniform beam at the isocentre into a clinically useful beam through a combination of attenuation at the centre of the beams and scatter at the periphery of the beam. The flattened beam will pass through dual ion chambers located below the filtering filter to monitor the integrated dose, dose rate and beam quality of the beam. The ion chambers are sealed to prevent the external interference such as temperature, pressure and humidity of the outside air could influence their response. The dose is measured in monitor unit (MU), which depends on the reference dose rate usually 1.0 cGy/MU at a linac calibration point (Almond et al., 1999). The ion chamber also monitors the beam characteristics and the dose delivered. The linac will stop the beam delivery if the beam characteristics exceeded the acceptance level or the dose has been delivered as prescribed. Below the ion chamber, there is a motorised wedge that has a thick and a thin ends. The thin end causes less attenuation than the thick end. The wedge function is to shift the isodose curve within the treated volume if necessary based on the desired dose distribution.

The beams are shaped by another set of collimators to deliver a more conformal beam to the tumour. A conventional linac shapes the beam by a set of dense metal collimators built in the machine, known as jaws. These collimator jaws are frequently used with the secondary customised beam blocks that are attached to the linac below the collimator jaws for beam shaping purposes.

The fabricated blocks have a range of shapes and sizes for a given field applied to a specific patient. However, the conventional method restricts the conformity of the beam as it only allows limited number of beam shape. Multileaf collimator (MLC) has now replaced the beam blocks for shaping the beam. MLC is composed of movable leaves that can drive automatically and independent of each other to generate a field of any shape and size. The design and operating principles of MLC will be further explained in Section 3.2.1.

2.1.2 Electronic portal device (EPID)

Historically, megavoltage (MV) images have been acquired with radiographic film designed specifically for portal imaging. Film has long been considered the gold standard in imaging, offering high resolution and provide adequate image quality for radiotherapy information. However, there are several limitations that lead to the replacing of film for treatment imaging, such as time consuming film exposure and development time. The delay makes the portal film imaging impractical during the treatment, in which the information is no longer valid due to patient movement or internal organ motion. In the last few decades, the EPID has started to become more widely available and replacing the films for a faster verification purpose (Herman et al., 2001).

EPID is mounted on the gantry opposite the treatment head to allow acquisition of images of the beam delivery. EPID has been used for patient positioning verification during the treatment and used as quality assurance tool to check the several radiotherapy linac parameters such as MLC positional accuracy.

The current generation of EPID is known as amorphous silicon (a-Si) array detector. The array detector is comprised of a thin metal plate (typically copper) which acts as build up for the primary beam and filters for low energy scattered photon and electrons, a phosphor screen (such as terbium-doped gadolinium oxysulfide, $Gd_2O_2S:Tb$ (Gadox)) to convert x-rays into lights, a light

sensor (such as a-Si photodiode) to detect the light and the associated readout electronics. The schematic drawing of components in an a-Si EPID system is shown in Figure 2.3. The main principle of an a-Si EPID is based on two step processes. In the first step, the incident x-rays are converted into optical photons by means of metal plate and the phosphor screen. In the second step, the generated photons are absorbed by the a-Si photodiode which create electrical signal (Blake et al., 2013).

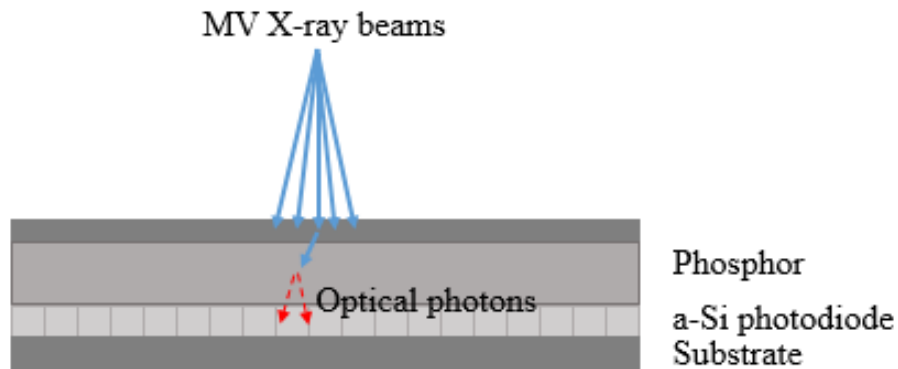


Figure 2.3 Schematic diagram of cross-section of an a-Si EPID (Blake et al., 2013)

2.1.3 CBCT imaging system

The CBCT imaging system consists of a kilovoltage x-ray tube and a flat panel detector. The x-ray tube is a glass enveloped containing a cathode assembly (negative electrode) and an anode assembly (positive electrode). Figure 2.4 shows a schematic illustration of the components an x-ray tube that is connected to power supply. The tungsten filament ejects electrons when it is heated by passing through an electric current. A cloud of electrons will form around the filament as it is heated up to approximately 2200° C.

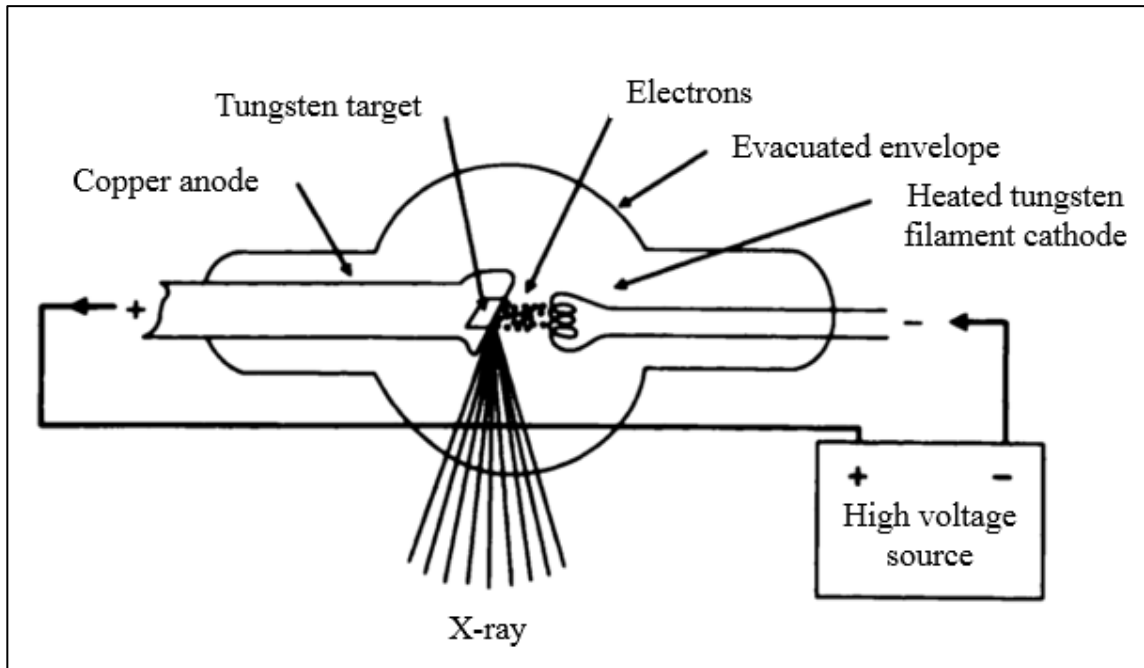


Figure 2.4 X-ray tube and its power supply (Bushberg et al., 2011)

The x-ray tube current (mA) is determined by the number of accelerated electrons per second, which is 1 mA equal to 6.24×10^{15} electrons/sec (Bushberg, et al., 2011). Moreover, the amount of energy gained by the electrons is determined by the potential difference between cathode and anode. For example, the energy of electron with applied potential of 120 kV will reach the anode at 120 keV. The maximum energy gained by electron can be defined by peak voltage (kVp). The number of accelerating electrons from cathode to the anode increase proportionally to the tube current (mA) as well as the exposure time (s). Changing both parameters will alter the number of x-ray beams produced at a specific energy.

The vacuum between cathode and anode, maintained by the envelope, and the high potential difference applied across the cathode and anode (20 to 150 kV), enabling electrons to be accelerated with a velocity of around half of the speed of light from cathode and collide at the target area of the anode. The collision produced the x-rays. There are two type of x-rays produced: bremsstrahlung and characteristic x-rays. A typical x-ray spectrum of both types of x-rays are

shown in Figure 2.5. The Coulomb interactions between the incident electrons and the target nuclei of the anode results in continuous x-rays radiation called bremsstrahlung x-rays. This type of radiation covers the entire range of the energy spectrum and is the dominant x-ray production process (Kruth et al., 2011). Meanwhile, the characteristic x-rays is produced as a result of collision between incident electrons with an orbital electron of the anode. The collision caused both electrons to be ejected from the target atom leaving a hole in the inner shell. The vacancy causes electron from the outer shell to occupy the inner shell. As a result, an x-ray of discrete with energy that is equal to the difference in the binding energies of the two electron shells is emitted. This characteristic x-ray is a property of the target material.

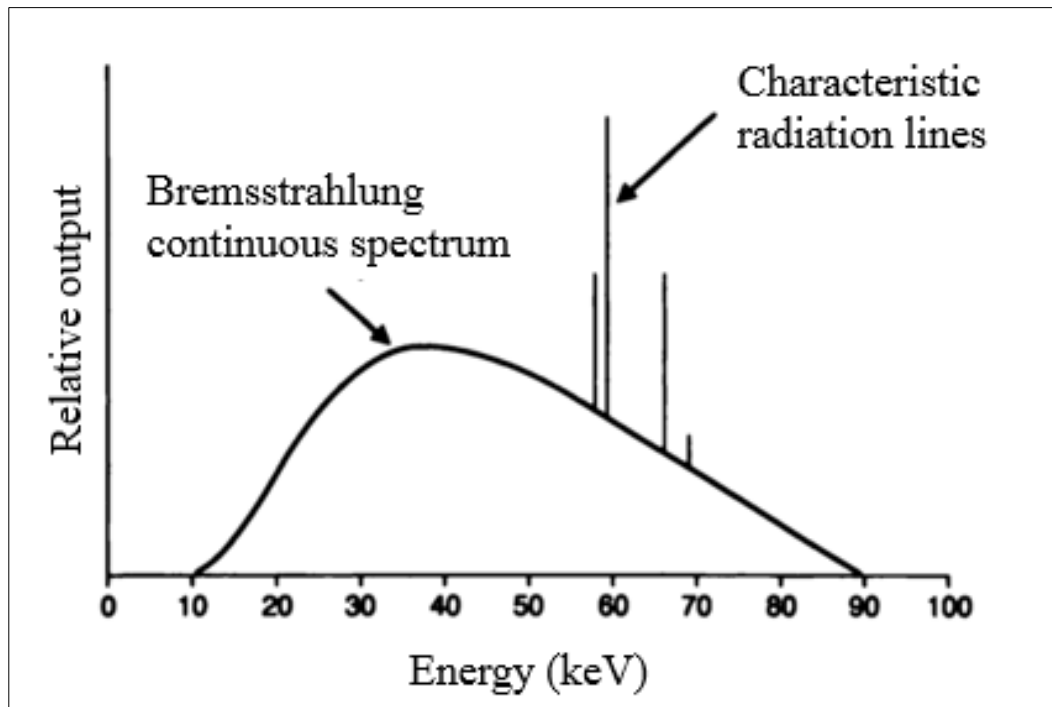


Figure 2.5 Typical x-ray spectra (Bushberg et al., 2011)

The x-ray beam produced a cone shaped beam, which can be filtered and reshaped by using different types of filters and collimator (Bushberg et al., 2011; Carlton et al., 2013). The filters and collimators used in this project will be further explained in the Section 3.2.2. The x-ray

beams travel through a patient. The x-ray beams which are not absorbed by the target are differ in the x-ray intensity, which is dependent upon the area where they pass through. These variations in the intensity will be detected by the image receptor and create radiographic images. The image receptor is commonly a flat panel detector (FPD) that are generally composed of an a-Si array detector and a scintillator. The process of x-rays beam detection and image construction similar in the EPID.

2.2 Components of QAP for IGART

The goal of IGART is to optimise the ratio of normal tissue sparing and target coverage by adapting treatment plan throughout the treatment course. There are three main components in the implementation of IGART treatment: dose verification, image guidance, and plan adaptation (Wu et al., 2011). Therefore, QA tests should be performed and optimised with respect to these components: verification of the intensity modulated beam delivery (includes monitoring of linac dose output and MLC performance) and the performance of the image guidance system for adaptation. Relevant components in QAP for IGART are summarised in Table 2.1. The QA test protocols for linac dose output, MLC and image guidance system will be explained in Section 2.2.1, 2.2.2, and 2.2.3, respectively.

Table 2.1 Relevant QAP for IGART

Components	Frequency of test	Metrics
Linac dose output	Daily	<ul style="list-style-type: none"> • Dose output • Beam profile • Beam energy
	Monthly	<ul style="list-style-type: none"> • Central dose output • Beam energy
MLC radiation shaping	Weekly	<ul style="list-style-type: none"> • MLC positional accuracy
CBCT image guidance	Monthly	<ul style="list-style-type: none"> • Noise and uniformity
		<ul style="list-style-type: none"> • Contrast: contrast to noise ratio (CNR) and low contrast visibility (LCV)
		<ul style="list-style-type: none"> • Spatial resolution
		<ul style="list-style-type: none"> • Geometric distortion • CT number

2.2.1 Linac dose output

The linac dose output should be measured daily and monthly in accordance to TG-40 (Kutcher et al., 1994) and TG-142 (Klein et al., 2009) recommendations. Typically, a water tank phantom and an ionisation chamber (calibrated against secondary standard dosimetry laboratory (SSDL)) are used for beam measurement during commissioning as recommended by TG-106 (Das et al., 2008). However, the setup is complex and time consuming. Hence, a more simple and efficient setup device can be used during the routine measurements of daily and monthly tests. For example, a secondary measurement system is used for monthly measurements and tertiary system is used for daily measurements as a consistency check. In fact, these systems should be appropriately used and calibrated against the absolute standard data (Smith et al., 2017). The absolute data

measurement commonly followed AAPM TG-51 (Almond et al., 1999) or IAEA TRS-398 (IAEA, 2000) recommendations.

The tolerance levels of linac dose output constancy suggested by AAPM TG-40 and TG-142 are different based on the test frequencies. For daily measurements, the linac dose output should fall within $\pm 3\%$ of baseline, and for monthly measurements should fall within 2% of baseline. Meanwhile, IAEA Report 31 has recommended the linac output constancy uncertainties of $\pm 2\%$ (IAEA, 2016). Besides, survey done by Palmer et al. (Palmer et al., 2012) and Bolt et al. (Bolt et al., 2017) to determine current radiotherapy linac quality control practice in many centres found that the allowable range of dose output set by most of the centres is $\pm 2\%$. An action to correct the linac dose output should be taken if the dose output is outside of the tolerance level to bring back to an acceptable level.

Another important quantity that should be measured to ensure the accuracy and reproducibility of dose delivered from the linac is constancy of the beam profile. It is measured in term of beam flatness and beam symmetry (Klein et al., 2009; Kutcher et al., 1994). The recommendation of tolerance level for monthly measurements is $\pm 2\%$ (Klein et al., 2009; Kutcher et al., 1994; Smith et al., 2017). The beam energy constancy also plays an important role in ensuring the accuracy and reproducibility of dose delivery in radiotherapy. During data commissioning, the full depth dose curve in water is measured as percentage depth dose (PDD). PDD is an attenuation-based metric which traditionally used to monitor the beam energy (Klein et al., 2009; Kutcher et al., 1994). The routine measurement should verify that the PDD curve does not deviated from the commissioning result. Tissue phantom ratio (TPR) is introduced as a simplified version of PDD to describe the changes in dose with depth that usually measured at two depth points in water (Purdy, 1977). AAPM TG-51 and IAEA TRS 398 have provided guidelines to perform the TPR measurement. The tolerance level of beam energy is $\pm 1\%$ of the PDD (Klein et al., 2009; Smith et al., 2017).

Most of the daily devices (will be explained further in Section 3.3.2) are now designed capable to measure other beam parameters besides dose output including the beam flatness, the beam symmetry and the energy constancy. The daily results of the parameters can be monitored daily and verified against the monthly standard methods.

2.2.2 Multileaf collimator (MLC) radiation shaping

IMRT delivers highly conformal and complex dose distributions that utilise dynamic movement of the MLCs. The radiation dose is modulated to the target at different parts of target area. The dose is delivered with MLCs are continuously changing the shape without any beam hold-off in between the irradiation. In IGART, MLCs adjustments are the most common means to adapt the shape and size of tumours during the course of treatment (Yan, 2008). The study conducted by Wu et al. has shown that modifying treatment plan using MLCs resulted in better dose efficacy in terms of dose distribution in the target and in normal tissue of prostate and head and neck cancer treatment (Wu et al., 2006). Besides, the recent study conducted by Keall et al. also used the method of adjusting the leaf position to optimally align the treatment beam with real-time target position. Eight prostate stereotactic abative body radiotherapy (SABR) patients were treated with this real-time technique (Keall et al., 2018).

For the complex treatment fields, dose delivery throughout the target volume is sensitive to leaf positioning and leaf transmissions. This is supported by several publications that documented the impact of leaf positioning accuracy on the delivered IMRT fields such as (Bayouth & Morrill, 2003) and (LoSasso, 2008). Therefore, it is essential to routinely monitor the MLC performance to ensure the accuracy and reproducibility of the leaf motion in every fraction of the treatment plan (LoSasso et al., 2001).

According to TG-142 (Klein et al., 2009), the MLC performance tests should be conducted on weekly and monthly basis by delivering a beam that requires the MLCs to move dynamically, such as the picket fence test described by (LoSasso et al., 2001). Conventionally, the test used to assess leaf positional accuracy qualitatively by the matching of sequential segments and leaf transmission during the beam modulated by dynamic MLCs. For example, TG-142 suggested a careful examination of the image acquired by static film or EPID is performed to assess the MLC performance. The prescriptions of picket fence test is further explained in Section 3.4.1. On a monthly test, the leaf position accuracy test is expanded to account for gantry rotation which may affect leaf motion due to gravitational effects imposed on the leaf carriage system. TG 142 suggested MLC positional tolerance for monthly test is ± 1 mm. This is agreed by Budgell et al. where the accuracy of leaf positioning should be better than 1 mm to ensure accurate dose delivery of IMRT fields (Budgell et al., 2000b)

2.2.3 CBCT image guidance system

IGART highly relies on imaging guidance during the fractional beam delivery. A CBCT based image guidance is used for imaging and positioning. However, positioning accuracy is beyond the scope of this study. Thus, an effort should be taken in developing a QAP for the imaging device to ensure that the imaging performance characteristics do not differ from the established baseline at the time of commissioning (Klein et al., 2009). AAPM TG-179 (Bissonnette et al., 2012) has suggested several aspects of QAP (test and tolerance) to determine the performance of the CBCT system with respect to IGART requirements, such as image quality and accuracy of CT numbers. Image quality measurements in that report basically followed TG-74 (Whiting, 2002) and TG-142 (Klein et al., 2009). TG-179 recommends a set of image quality tests that is performed initially on a monthly basis, and ultimately on a semi-annual basis, after the stability of CBCT system has